Electronic structures of rocksalt, litharge, and herzenbergite SnO by density functional theory

Aron Walsh and Graeme W. Watson*
Department of Chemistry, Trinity College, Dublin 2, Ireland
(Received 16 March 2004; revised manuscript received 26 May 2004; published 13 December 2004)

Density functional theory calculations have been performed on SnO in the litharge, herzenbergite, and rocksalt crystal structures. An asymmetric electron distribution was found around the Sn atoms in litharge and herzenbergite SnO which could be ascribed to a Sn $5s^2$ sterically active "lone pair." Analysis of the electronic structure shows that the states responsible for the asymmetric Sn electron distribution are due to the coupling of unfilled Sn($5p$) with the antibonding combination arising from interaction of Sn($5s$) and O($2p$). The coupling of Sn($5p$) was found to be active in both the formation of the asymmetric density and the stabilization of the litharge and herzenbergite phases. Due to the symmetry of the interaction the coupling of Sn($5p$) with the antibonding states can only take place on distorted Sn sites, explaining the absence of an asymmetry in the rocksalt structure. In contrast to the classical view that the Sn(II) "lone pair" forms directly through hybridization of Sn $5s$ and $5p$, our calculations confirm for the first time, through COOP analysis, that it is only through the interaction of the oxygen $2p$ states that formation of the asymmetric density is achieved.

DOI: 10.1103/PhysRevB.70.235114 PACS number(s): 71.20.−b

I. INTRODUCTION

Many Sn(II) compounds exhibit interesting physical properties and possess numerous technological applications, with recent work being performed on the use of SnO nanoparticles in rechargeable batteries[1] and on SnS thin films for use in solar cells.[2] In Sn(II) compounds, Sn acquires an electronic configuration of $4d^{10}5s^25p^0$, with a filled $5s$ subshell. The classical view is that after hybridization of the s and p orbitals, the Sn $5s^2$ electrons occupy an inert orbital,[3] which is projected out one side of the Sn atom, creating an asymmetric structure. This inert pair of electrons is thus considered a lone pair,[4] and while they are deemed not active in bonding,[5] they are deemed to be sterically active, resulting in asymmetric crystal structures. However, this distortion is not present in all Sn(II) compounds, which would suggest the formation and stability of the lone pair is more complex than classical hybridization would imply.

Classical hybridization suggests that lone pairs would form for all Sn(II) compounds, hence it would be expected that all Sn(II) compounds adopt asymmetric structures, which is not the case. For example, the SnX (X=O, S, Se, and Te) series, while having similar electronic configurations exist in quite different crystalline environments. These range from highly symmetric SnTe which adopts the perfectly symmetric, six coordinate rocksalt structure, with a $Fm3m$ space group as its thermodynamically stable phase, Fig. 1(a), to highly distorted SnO. SnO assumes a layered tetragonal structure[6] (litharge) with a $P4/nmm$ space group, Fig. 1(b), containing asymmetric four coordinate Sn sites, that can be seen as a distortion of the eight coordinate CsCl structure. SnS and SnSe both adopt an intermediate orthorhombic structure[7] (herzenbergite) with a $Pnma$ space group, which can be seen as a distortion of the rocksalt structure creating asymmetric coordination around the three coordinate Sn atoms, Fig. 1(c).

Density functional theory (DFT) calculations on PbO[8] have suggested that the formation of the so-called "sterically active lone pair" and the stabilization of the distorted structures are not purely the result of the Pb $6s^2$ electrons. In a previous study[9] we performed DFT calculations within the local density approximation (LDA) on litharge and CsCl structured SnO, which again suggested that the formation of the "lone pair" and the stabilization of the litharge phase over the undistorted CsCl structure are not purely the result of the Sn $5s^2$ electrons. Both these studies indicate that O($2p$) is involved in the states responsible for the lone pair and that the cation ns^2 electrons are at least partially involved in chemical bonding with the oxygen.

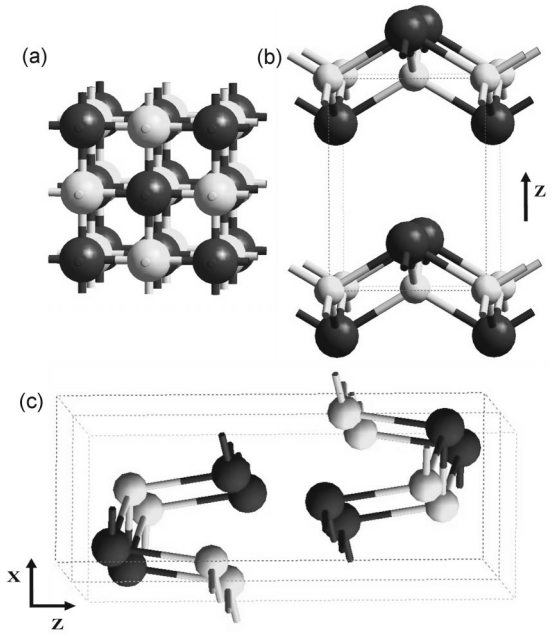

FIG. 1. Crystal structures of (a) rocksalt structured SnTe, (b) litharge SnO, and (c) herzenbergite SnSe. Sn atoms are colored dark, while the anion atoms are colored light.

TABLE I. Calculated structural properties of rocksalt, litharge, and herzenbergite SnO.

	Rocksalt	Litharge[a]	Herzenbergite
Energy (eV/Sn)	−10.52	−11.41	−11.22
Volume ($Å^3$/Sn)	33.48	37.25 (+6.1%)	39.70
a(Å)	5.116	3.867 (+1.7%)	11.784
b(Å)		3.867 (+1.7%)	3.403
c(Å)		5.036 (+4.1%)	3.950
Sn(z)		0.234 (−1.8%)	0.162
Sn-O (Å)	6×2.558	4×2.261 (+1.7%)	2×2.235
			1×2.754

[a]% error with respect to experimental data, Ref. 6.

DFT and tight binding calculations have been performed on the Sn(II) monochalcogenides by Lefebvre *et al.*,[10] although their emphasis was not on lone pair formation. The electronic structures were calculated in their observed crystalline structure only, preventing a full analysis of Sn(II) lone pair behavior. While more recent calculations have been performed on ns^2 lone pairs in Ge, Sn, and Pb chalcogenides using DFT and electron localization functions,[11] this study mainly addresses the compounds in the rocksalt structure, which restricts their investigation of lone pair formation seen in asymmetric structures. This leaves the precise mechanism behind the formation and stability of these lone pairs to be addressed. The aim of this work is to study the nature of the Sn(II) electron distribution in SnO, with emphasis on the formation of the asymmetric density, by the examination of the electronic structure of SnO in the litharge, herzenbergite, and rocksalt structures, the thermodynamically stable phases of the Sn monochalcogenide series. Electronic structure analysis of SnO in each of the three crystal structures will give a better understanding of the origin of the electron distribution in Sn(II) materials.

II. COMPUTATIONAL METHODS

Our electronic structure calculations were performed using DFT as implemented in the Vienna *Ab-initio* Simulation Package[12–14] (VASP). The exchange and correlation energy is evaluated within the generalized gradient approximation (GGA) using the parametrization of Perdew *et al.*[15] Three dimensional periodic boundary conditions were employed which allow the expansion of the crystal wave functions in terms of a plane wave basis set. The projector augmented wave method[16,17] (PAW) was used to treat the core electrons (Sn: [Kr], O: $1s^2$), as it keeps the computational efficiency of a pseudopotential by substantially reducing the number of plane waves required, while retaining the accuracy of a fixed core all electron calculation.

The forces on the atoms and the stress tensor were calculated using the Hellman-Feynman theorem. These were used to perform constant volume quasi-Newton relaxations until the forces on the atoms had converged to less than 0.001 eV/Å, and the pressure on the cell had equalized. Convergence of the total energy was checked with respect to both the plane wave cutoff energy and k-point density, which were obtained using the Monkhorst-Pack method.[18] A plane wave cutoff of 500 eV was used with k-points grid sizes of $8\times8\times8$ for the two atom, reduced unit cell rocksalt structure and $6\times6\times4$ and $4\times6\times6$ for litharge and herzenbergite structures, respectively.

III. RESULTS

A. Optimization of the lattice vectors

Each of the three structures (rocksalt, litharge, and herzenbergite) were optimized by performing a series of calculations at different volumes. In each of these the length and angles of the lattice vectors and the atom positions are optimized within the constraint that the total volume does not change. The resulting energy volume curve was fitted to the Murnaghan equation of state[19] to obtain the equilibrium cell volume. Optimization at this volume yields the equilibrium structures and binding energies shown in Table I. The litharge structure is predicted to be the most energetically favorable as would be expected for the thermodynamically stable phase. The herzenbergite structure is predicted to be only 0.19 eV/Sn less favorable, with the cubic rocksalt phase being the highest energy SnO structure, 0.89 eV/Sn less stable than the litharge phase.

The predicted a and b lattice vector and the internal coordinate for the litharge structure are in good agreement with experimental values.[6] The a and b lattice vector is slightly overestimated in our calculations, in the order of 2%, which is a general feature of GGA-DFT calculations. However, the c vector, which represents the Sn-O layer interactions, is overestimated to a greater extent due to the relatively weak nature of the forces in this direction which are poorly described in DFT. The rocksalt structure is calculated as having six oxygens coordinated 2.558 Å from Sn, while the Sn-O distances for the litharge phase are calculated to within 2% of the experimental values at 2.261 Å. The herzenbergite phase is calculated as having one long 2.754 Å and two short 2.235 Å Sn-O interatomic distances, in contrast to the two long and one short seen for the herzenbergite SnS and SnSe. This corresponds to an elongated c vector in the unit cell, which is caused by the Sn atoms moving along the c vector, and is most likely a result of stronger lone pair activity in SnO compared with SnS and SnSe.

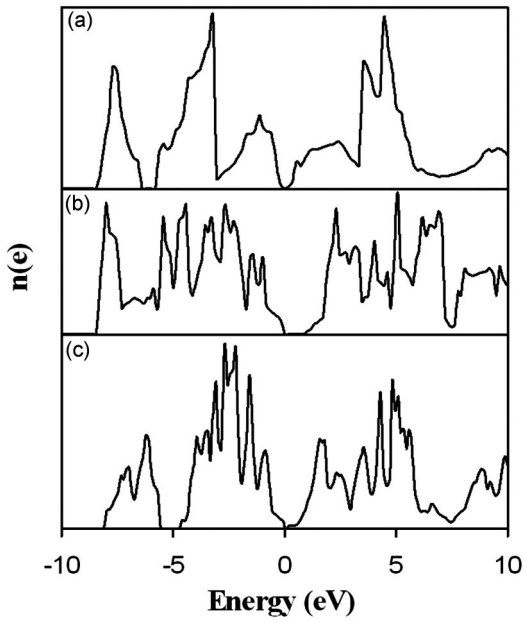

FIG. 2. Total electron density of states from −10 eV to +10 eV for (a) rocksalt, (b) litharge, and (c) herzenbergite SnO, relative to the highest occupied state of each structure.

B. Electron density of states

The electron density of states (EDOS) for the three structures are shown in Fig. 2 from −10 eV to +10 eV (with respect to the highest occupied state). While the O(2*s*) and Sn(4*d*) states both occur at lower energies they have no significant role in bonding and have therefore been excluded for clarity. The EDOS possess a number of common features. The area below the Fermi level can be divided into three main regions. The lowest energy region (region I) from −9 eV to −6 eV, the second region (region II) from −6 eV to −3 eV, and the third region (region III) from −3 eV to the highest occupied state. The EDOS of the rocksalt structure reflects its symmetric nature and contains well-defined peaks unlike the asymmetric litharge and herzenbergite structures, which appear more complex.

A number of differences are notable between the EDOS of the three structures. The litharge phase features substantial overlap between the peaks in regions I and II, in contrast to the rocksalt and herzenbergite structures. In addition, while containing a distinguishable central peak in the rocksalt and herzenbergite phases, region II of the litharge structure displays a much broader distribution of states, forming extensive overlap with region III. Region III, situated just below the Fermi level contains a single peak centered at −1 eV in the rocksalt structure but appears split and shifted down to −1.5 eV in the herzenbergite structure. While the overlap between regions II and III partly conceals the region III peak of the litharge structure, these states are clearly shifted down in energy, relative to the other structures, centered at approximately −2 eV. The unoccupied states of litharge and herzenbergite SnO are also shifted away from the Fermi level giving rise to the larger band gaps of 1.148 eV and 0.520 eV for these structures compared to semimetallic rocksalt SnO. The experimentally determined value of between 2.5 eV and 3 eV for litharge SnO[20] shows that our calculated band gaps are significantly underestimated, a well known failing of DFT.

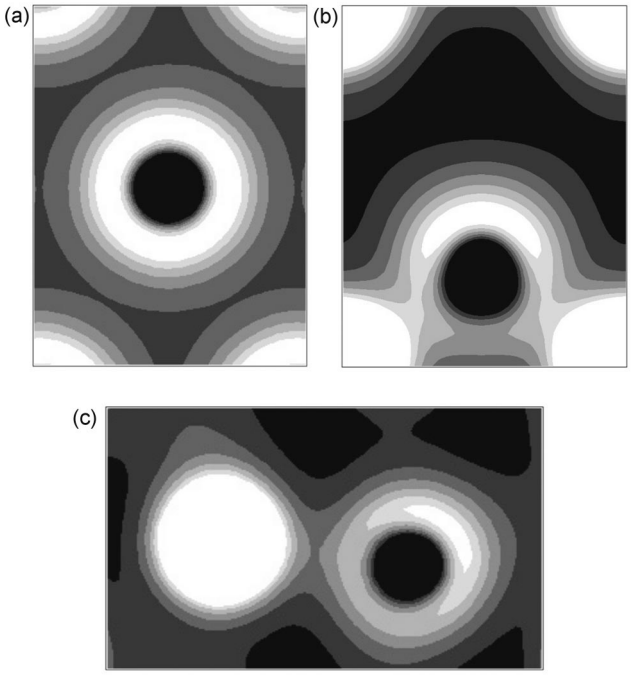

FIG. 3. Electron density contour plots through a plane containing Sn atoms for (a) rocksalt, (b) litharge, and (c) herzenbergite SnO. Contour levels shown are between 0 $e/\text{Å}^3$ (black) and 0.35 $e/\text{Å}^3$ (white).

C. Electron densities

The electron densities from the states between 0 eV and −9 eV (with respect to the highest occupied state), through a plane containing Sn atoms, for rocksalt, litharge, and herzenbergite SnO are shown in Fig. 3, with black and white showing regions of low and high electron density, respectively. For the rocksalt phase, the electron density around the Sn atoms is clearly spherical. In contrast, litharge and herzenbergite SnO form an enhanced density to the side of the Sn atoms pointing away from the Sn-O layers. Traditionally this asymmetric electron density would be attributed to a lone pair with the Sn $5s^2$ electrons occupying a *sp* hybridized orbital, which would be interpreted as being stereochemically active in directing the layered structures.

To establish the region from which the lone pair originates, partial electron density maps were made for the three regions of the EDOS, an example of which is shown for litharge SnO, Fig. 4. Figure 4(a) displaying the density arising from region I of the EDOS clearly shows the formation of an enhanced density between O and Sn, indicating a bonding interaction between the anion and cation which does not contribute to the lone pair. Region II is shown to be mainly oxygen in nature, Fig. 4(b), and again does not directly contribute towards an asymmetric Sn electron distribution. The Sn lone pair is clearly due to electron density originating

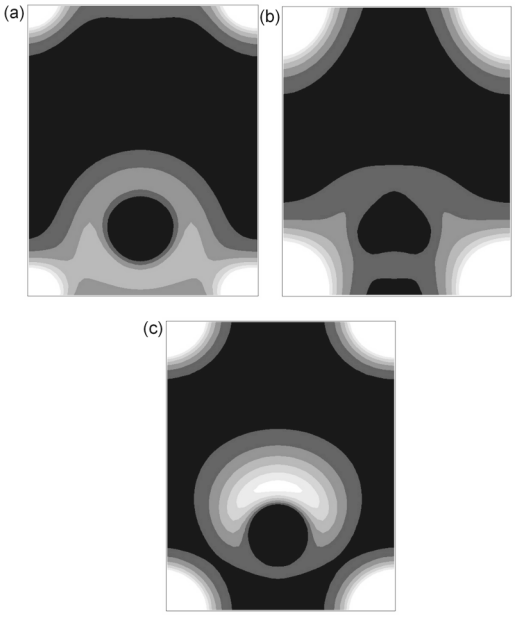

FIG. 4. Partial electron density contour plots for litharge SnO. Contour levels shown are between 0 $e/\text{Å}^3$ (black) and 0.25 $e/\text{Å}^3$ (white). (a) −9 eV to −6 eV, (b) −6 eV to −3eV, and (c) −3 eV to 0 eV.

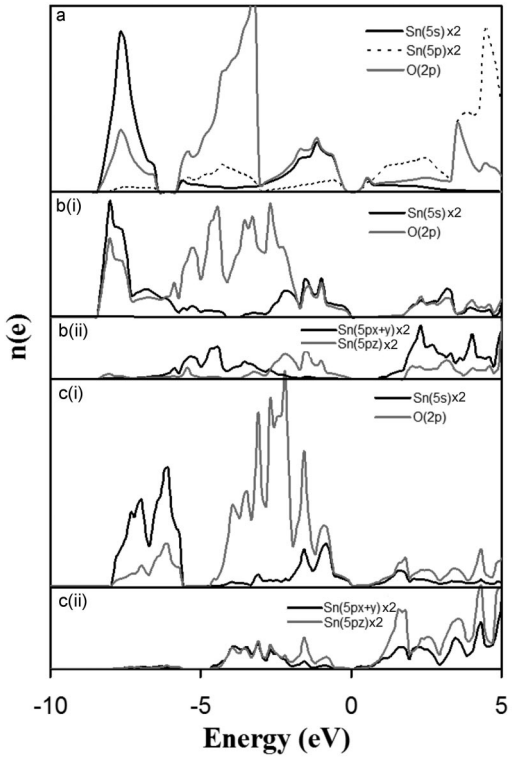

FIG. 5. Partial electron density of states for (a) rocksalt (b) litharge, and (c) herzenbergite SnO, relative to the highest occupied state in each structure. The Sn 5*s* and 5*p* states have been doubled in each case for clarity.

from region III of the EDOS, Fig. 4(c). A spherical electron distribution can be seen around the O atoms with an enhanced density present above the Sn atom, pointing away from the Sn-O layer. The density between the O and Sn atoms can be seen to fall close to zero in this region which suggests an antibonding Sn-O interaction.

D. Partial electron density of states

To aid the interpretation of the electronic structure, in addition to the EDOS we have also calculated the partial (ion and *l*- and *m*-quantum number decomposed) electronic density of states (PEDOS) for all three structures. These were obtained by projecting the wave functions onto spherical harmonics centered on each atom with a radius of 1.55 Å for Sn and 1.55 Å for O.[21] The radii chosen give rise to reasonable space filling and the results are qualitatively insensitive to changes in radii. Figure 5 shows the PEDOS curves from −10 eV to +5 eV for both Sn and O in the rocksalt, litharge, and herzenbergite structures.

The PEDOS show that region I is a mixture of Sn(5*s*) and O(2*p*) states, with regions II and III mainly O(2*p*) in nature. This is broadly in line with an ionic model of SnO in which the two Sn(5*p*) electrons have been transferred to O(2*p*). However detailed examination reveals a more complex system exists. Region I of the litharge and rocksalt phases consists of approximately 50% Sn(5*s*) and 50% O(2*p*) character, while this region in herzenbergite SnO contains approximately 60% Sn(5*s*) character, which is perhaps due to the lower coordination of the structure. Region II is almost completely O(2*p*) in nature, containing only small amounts of Sn(5*p*) states. Region III consists of approximately 70% O(2*p*), 25% Sn(5*s*), and 5% Sn(5*p*) character in the rocksalt phase, 50% O(2*p*), 28% Sn(5*s*), and 22% Sn($5p_z$) character in litharge SnO, and 70% O(2*p*), 18% Sn(5*s*), and 12% Sn($5p_z$) in the herzenbergite structure. The asymmetric structures both contain significant amounts of Sn($5p_z$) in region III, with the Sn($5p_z$) character of the litharge structure almost equaling that of the Sn(5*s*) character. Also of note is the fact that the litharge structure contains less O(2*p*) states close to the Fermi level than the two less stable structures. As has been illustrated through electron density contour maps it is region III that is responsible for the asymmetry in the Sn electron density and so these differences are directly related to the so-called "lone pair."

From the PEDOS it is evident that region III contains less than one-third of the overall Sn(5*s*) states with the majority being present in region I. The overlap that exists between the Sn(5*s*) and O(2*p*) states in regions I and III would again suggest that these regions correspond to the combinations arising from a Sn(5*s*) and O(2*p*) interaction occurring in all structures. However, in addition the PEDOS of asymmetric litharge and herzenbergite SnO contain a number of features that are not present in the symmetric rocksalt structure. Most notable is the presence of Sn($5p_z$) states in region III of the PEDOS, directly overlapping with the Sn(5*s*) and O(2*p*) peaks. These structures also contain additional unoccupied, overlapping Sn(5*s*), Sn($5p_z$), and O(2*p*) peaks, situated above the Fermi level at approximately +1.5 eV in the herzenbergite structure and +3 eV in the litharge structure. This would suggest that additional interactions occur in the

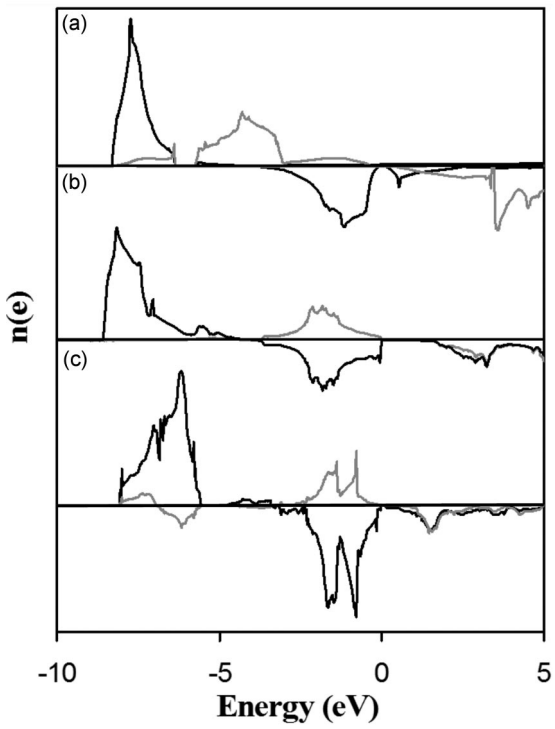

FIG. 6. Crystal orbital overlap populations for the Sn(5*s*) -O(2*p*) (black) and O(2*p*)-Sn(5p_z) (grey) interactions in the (a) rocksalt, (b) litharge, and (c) herzenbergite structures.

asymmetric structures which result in the unoccupied peaks observed. Of particular interest is Sn(5*s*) which does have any significant peaks above the Fermi level in the rocksalt structure.

E. Crystal orbital overlap populations

To examine the nature of the interactions suggested by the PEDOS, the crystal orbital overlap populations[22] (COOP) for the Sn(5*s*)-O(2*p*) and Sn(5p_z)-O(2*p*) interactions have been calculated for all three structures and are shown in Fig. 6. The COOP represents the bonding between two orbital centers. It is a density of states weighted overlap population ($2c_1c_2S_{12}$), where the overlap integral, S_{12}, is taken as a positive value. Therefore positive and negative regions signify bonding and antibonding interactions, as the direction of the COOP is determined by the signs of the coefficients.

The Sn(5*s*)-O(2*p*) and Sn(5p_z)-O(2*p*) interactions contain contributions from both O(2p_y) and O(2p_z) states. The latter interaction only takes into account Sn(5p_z) as this is the dominant interaction, although additional Sn(5p_y) and Sn(5p_z) interactions can be seen to occur for the herzenbergite phase, arising from the orientation of the Sn atoms in the unit cell. The Sn(5*s*)-O(2*p*) COOP (black lines) for each structure result in a large positive peak from −9 eV to −6 eV and a large negative peak from −3 eV to the highest occupied state. This shows that an interaction takes place between the Sn(5*s*) and O(2*p*) states which results in filled bonding and antibonding combinations in regions I and III, respectively. The negative region III peak confirms that it is composed of filled antibonding states. The difference between the three structures comes in the size and position of the antibonding combination. The antibonding peak is smallest and positioned lowest in energy for litharge SnO at −2 eV. A larger split peak is present at −1.5 eV for the herzenbergite structure, with the peak for rocksalt SnO being the largest and positioned highest in energy at −1 eV.

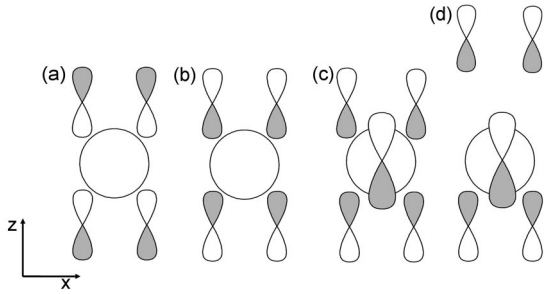

FIG. 7. Schematic representation of orbital interactions for the (a) bonding and (b) antibonding Sn(5*s*)-O(2*p*) combinations and the interaction of Sn(5p_z) with the antibonding combination in both (c) symmetric and (d) asymmetric crystal structures.

The Sn(5p_z)-O(2*p*) COOP (grey lines) show no significant interaction in region III for the rocksalt phase. A bonding interaction can be seen to occur between the O(2*p*) and Sn(5p_z) in region II for this structure which bears no relation to the antibonding Sn(5*s*)-O(2*p*) states and hence does not effect lone pair formation. For the distorted litharge and herzenbergite structures the Sn(5p_z)-O(2*p*) COOP produces a positive peak in region III and a negative peak positioned above the Fermi level. This shows that in these structures an interaction between the O(2*p*) and Sn(5p_z) states results in a bonding region III combination and an unoccupied antibonding combination positioned at +3 eV in litharge SnO and at +1.5 eV in the herzenbergite phase. The symmetric Sn sites in the rock-salt structure do not allow for the region III Sn(5p_z)-O(2*p*) interaction which occurs in both asymmetric structures. It can be seen that for litharge and herzenbergite SnO the antibonding states produced from the Sn(5*s*)-O(2*p*) interaction directly couple with Sn(5p_z) states present in region III. This interaction is consistent with the presence of an additional Sn(5p_z) peak in region III of the EDOS and a Sn(5*s*) peak present above the Fermi level in the PEDOS of the litharge and herzenbergite structures. The filling of the bonding Sn(5*p*) states also help explain the stabilization of the antibonding Sn(5*s*)-O(2*p*) peak seen for the distorted phases.

These interactions are explained schematically for the Sn(5*s*)-O(2p_z) and Sn(5p_z)-O(2p_z) interactions using orbital diagrams, Fig. 7. The out of phase O(2*p*) orbitals have been suggested from band structure calculations on PbO,[23] which indicate that the Pb(6*s*)—O(2*p*) interactions are strongest when neighboring cells have opposite phases. The bonding and antibonding interactions of Sn(5*s*) and O(2*p*) are shown in Figs. 7(a) and 7(b), respectively for symmetric Sn coordination. These two interactions alone clearly cancel each other out and could not result in formation of an asymmetric density. As illustrated by Fig. 7(c), the out of phase O(2*p*)

orbitals restricts any coupling of Sn($5p_z$) with the antibonding Sn($5s$)-O($2p$) combination. While this interaction is in phase on one side of the Sn($5p$) orbital, the out of phase interaction on the opposite side results in no net interaction. However, the displacement of the Sn atoms in a distorted structure breaks this symmetry, Fig. 7(d). As the Sn sites are distorted, only the in phase interaction remains, making the interaction of Sn($5p_z$) with the antibonding combination viable.

The Sn electron density is enhanced through constructive interference of Sn($5s$) and Sn($5p_z$) on one side of the Sn atom, away from the oxygen atoms, which as can be seen in the region III partial electron density map, Fig. 4(c), results in the formation of the observed asymmetric density in the distorted structures. The Sn electron density is thereby reduced through destructive interference on the opposite side of the atom where the oxygen atoms are. This stabilizes the high energy states by effectively reducing the antibonding interaction with O($2p$).

IV. DISCUSSION

The complexity of the EDOS for each structure shows a mixing of states that is not predicted by a simple ionic model of SnO. The region identified as being responsible for the lone pair in SnO using partial electron density plots was found to contain less than one-third of the overall Sn($5s$) states. Examination of the PEDOS and COOP revealed this region (region III) to consist of the filled antibonding combination arising from a Sn($5s$)-O($2p$) interaction which occurred in all structures. However, as illustrated with the orbital diagrams, if region III was merely the filled antibonding combination of the Sn($5s$)-O($2p$) interaction this would cancel the effect of the bonding interaction in region I and since both of these states are symmetric, no asymmetry in the Sn electron density would result. This occurs for SnO in the rocksalt structure, with the bonding and antibonding combinations from the interaction clearly present in regions I and III of the PEDOS, but no asymmetric density is produced.

Further PEDOS and COOP analysis shows that for the litharge and herzenbergite structures additional coupling of Sn($5p_z$) with the filled antibonding Sn($5s$)-O($2p$) states occurs. This interaction, which is seen only to take place in structures with distorted Sn sites, results in filled bonding and empty antibonding combinations. The asymmetric Sn electron density is produced through constructive interference of Sn($5s$) and Sn($5p_z$) and stabilization is achieved as a result of the Sn($5p_z$) orbital shifting density away from oxygen, reducing the antibonding Sn($5s$)-O($2p$) combination. This can be seen in the PEDOS of the asymmetric structures where the near Fermi level states appear shifted to lower energies relative to the undistorted rock salt structure. This explains the mixing of Sn($5p_z$) into region III of the EDOS and the presence of additional overlapping Sn($5s$), Sn($5p_z$) and O($2p$) peaks above the Fermi level in the distorted phases. In order to make the asymmetric structures energetically favorable the coupling of Sn($5p_z$) must be strong enough to make up for the lost coordination of the undistorted structure.

In summary our calculations show that the asymmetric Sn electron density found in the litharge and herzenbergite structures is produced through the coupling of the Sn($5p_z$), Sn($5s$), and O($2p$) in region III of the EDOS. The anion is directly involved in the interactions. The states close to the Fermi level producing the asymmetric density are 50% O($2p$), 22% Sn($5p$), and 28% Sn($5s$) in litharge with the majority of Sn($5s$) character present in the bonding states at lower energy. This would suggest that anions with different valence states may be unable to interact in the same way as oxygen. Work is currently underway calculating the electronic structure of the SnX series (X=O, S, Se, and Te), to investigate if changes in these interactions can be used to explain the unusual crystallographic changes seen along the Sn(II) monochalcogenide series.

V. CONCLUSIONS

The electronic structure of SnO has been calculated and examined using density functional theory in the litharge, herzenbergite, and rocksalt structures. The calculations show good reproduction of experimental results for litharge structured SnO. A spherical electron distribution was found around the Sn atoms in the rocksalt structure, while an asymmetric density was found around the Sn atoms in the distorted litharge and herzenbergite structures. Examination of the EDOS showed that the asymmetric density originated from states in the −3 eV to 0 eV region. This region was identified by COOP and PEDOS analysis to consist of the antibonding combination arising from an interaction between the Sn($5s$) and O($2p$) states, and to contain approximately 30% of the overall Sn($5s$) character. However, this interaction alone does not produce an asymmetric density as demonstrated for the rocksalt structure.

Further examination revealed an additional coupling between Sn($5p_z$) and the antibonding Sn($5s$)-O($2p$) combination which occurred in the litharge and herzenbergite structures. This coupling of Sn($5p$) was found to be responsible for the creation of the asymmetric density and the enhanced stability of the distorted Sn structures. Due to the symmetry of the interaction this coupling is only possible in structures with asymmetric Sn sites.

Our calculations show that the lone pair effect is not the result of a nonbonding lone pair. The driving force for the asymmetry is the bonding between Sn and O with the asymmetry resulting from the antibonding states. It is clear from our results that the anion plays a crucial role in the formation of the asymmetric Sn density as it is only through the interaction of Sn($5s$) and O($2p$) that the coupling of Sn($5p$) can take place. The fact that this interaction is not possible in structures with symmetric Sn sites explains the absence of an Sn(II) asymmetric density in the rocksalt structure. These results have implications for all materials with ns^2 electronic configurations. The occurrence of asymmetry within these materials will depend on the particular cation-anion interactions present. To examine this

effect future calculations will consider the SnX series (X=O,S,Se,Te).

ACKNOWLEDGMENTS

The authors would like to acknowledge the HEA for a PRTLI (Cycle III) grant, TCD for a Trinity College Postgraduate Studentship and Compaq and JREI (JR99BAPAEQ) for funding to purchase and support a 20 processor Compaq SC cluster at the Rutherford Appleton Laboratory. The authors would also like to thank Dr. Peter Oliver at RAL for access and assistance with Hrothgar, a 16 node Beowulf cluster.

*Electronic address: watsong@tcd.ie

[1] A. Odani, A. Nimberger, B. Markovsky, E. Sominski, E. Levi, V. G. Kumar, M. Motiei, A. Gedanken, P. Dan, and D. Aurbach, J. Power Sources **119**, 517 (2003).
[2] K. Takeuchi, M. Ichimura, E. Arai, and Y. Yamazaki, Sol. Energy Mater. Sol. Cells **75**, 427 (2003).
[3] L. E. Orgel, J. Chem. Soc. **1959**, 3815 (1959).
[4] I. Lefebvre, M. Lannoo, G. Allan, A. Ibanez, J. Fourcade, J. C. Jumas, and E. Beaurepaire, Phys. Rev. Lett. **59**, 2471 (1987).
[5] I. Lefebvre, M. Lannoo, J. Olivier-Fourcade, and J. C. Jumas, Phys. Rev. B **44**, 1004 (1991).
[6] J. Pannetier and G. Denes, Acta Crystallogr., Sect. B: Struct. Crystallogr. Cryst. Chem. **36**, 2736 (1980).
[7] A. S. Avilov, R. M. Imamov, and S. N. Navasardyan, Kristallografiya **24**, 874 (1979).
[8] G. W. Watson and S. C. Parker, J. Phys. Chem. B **103**, 1258 (1999).
[9] G. W. Watson, J. Chem. Phys. **114**, 758 (2001).
[10] I. Lefebvre, M. A. Szymanski, J. Olivier-Fourcade, and J. C. Jumas, Phys. Rev. B **58**, 1896 (1998).
[11] U. V. Waghmare, N. Spaldin, H. C. Kandpal, and R. Seshadri, Phys. Rev. B **67**, 125111 (2003).
[12] G. Kresse and J. Hafner, Phys. Rev. B **49**, 14251 (1994).
[13] G. Kresse and J. Furthmuller, Comput. Mater. Sci. **6**, 15 (1996).
[14] G. Kresse and J. Furthmuller, Phys. Rev. B **54**, 11169 (1996).
[15] J. P. Perdew, J. A. Chevary, S. H. Vorto, K. A. Jackson, M. R. Pederson, D. J. Singh, and C. Fiolhais, Phys. Rev. B **46**, 6671 (1992).
[16] P. E. Blöchl, Phys. Rev. B **50**, 17953 (1994).
[17] G. Kresse and D. Joubert, Phys. Rev. B **59**, 1758 (1999).
[18] H. J. Monkhurst and J. D. Pack, Phys. Rev. B **13**, 5188 (1976).
[19] F. D. Murnaghan, Proc. Natl. Acad. Sci. U.S.A. **30**, 244 (1944).
[20] J. Guerts, S. Rau, W. Ritcher, and F. J. Schmitte, Thin Solid Films **121**, 217 (1984).
[21] See EPAPS Document No. E-PRBMDO-70-107439 for a supplementary discussion of the projection radii. A direct link to this document may be found in the online article's HTML reference section. The document may also be reached via the EPAPS homepage (http://www.aip.org/pubservs/epaps.html) or from ftp.aip.org in the directory /epaps/. See the EPAPS homepage for more information.
[22] R. Hoffmann, *Solids and Surfaces* (Wiley-VCH, New York, 1988), p. 42.
[23] G. W. Watson, S. C. Parker, and G. Kresse, Phys. Rev. B **59**, 8481 (1999).